# Conformational sampling of membranes by Akt controls its activation and inactivation

Iva Lučić[a,b], Manoj K. Rathinaswamy[c], Linda Truebestein[a,b], David J. Hamelin[c], John E. Burke[c], and Thomas A. Leonard[a,b,1]

[a]Department of Structural and Computational Biology, Max F. Perutz Laboratories, 1030 Vienna, Austria; [b]Center for Medical Biochemistry, Medical University of Vienna, 1030 Vienna, Austria; and [c]Department of Biochemistry and Microbiology, University of Victoria, Victoria, BC, Canada V8W 2Y2

Edited by Philip N. Tsichlis, Tufts Medical Center, Boston, MA, and accepted by Editorial Board Member Peter K. Vogt March 16, 2018 (received for review September 14, 2017)

**The protein kinase Akt controls myriad signaling processes in cells, ranging from growth and proliferation to differentiation and metabolism. Akt is activated by a combination of binding to the lipid second messenger PI(3,4,5)$P_3$ and its subsequent phosphorylation by phosphoinositide-dependent kinase 1 and mechanistic target of rapamycin complex 2. The relative contributions of these mechanisms to Akt activity and signaling have hitherto not been understood. Here, we show that phosphorylation and activation by membrane binding are mutually interdependent. Moreover, the converse is also true: Akt is more rapidly dephosphorylated in the absence of $PIP_3$, an autoinhibitory process driven by the interaction of its PH and kinase domains. We present biophysical evidence for the conformational changes in Akt that accompany its activation on membranes, show that Akt is robustly autoinhibited in the absence of $PIP_3$ irrespective of its phosphorylation, and map the autoinhibitory PH–kinase interface. Finally, we present a model for the activation and inactivation of Akt by an ordered series of membrane binding, phosphorylation, dissociation, and dephosphorylation events.**

kinase | Akt | HDX-MS | SAXS | allostery

The protein kinase Akt/protein kinase B (PKB) plays critical roles in cell growth and survival, differentiation, and metabolism, as well as general cellular homeostasis (1). Hyperactivation of Akt is associated with cancer and tissue overgrowth disorders (2–5), while inactivation of Akt2 leads to insulin resistance in mice (6) and a severe form of inherited diabetes in humans (7). Akt is activated downstream of growth factor or hormone receptors that stimulate phosphatidylinositol-3-kinase (PI3K) activity at the plasma membrane (8). The product of PI3K, phosphatidylinositol-3,4,5-trisphosphate [PI(3,4,5)$P_3$], activates Akt by recruiting it to the plasma membrane, where it is phosphorylated on two sites in its kinase domain, T308 and S473, critical for its catalytic activity (9, 10). A third, constitutive, phosphorylation site at T450 in the turn motif is essential for Akt folding and stability (11).

We recently demonstrated the dependency on the signaling lipids PI(3,4,5)$P_3$ and PI(3,4)$P_2$ for Akt activation and activity in the cell (12). PI(3,4)$P_2$ is produced in the cell by class II PI3K (13), or by SHIP1/2-mediated hydrolysis of PI(3,4,5)$P_3$ (14), and, like PI(3,4,5)$P_3$, is capable of recruiting Akt to membranes via its PH domain (12, 15). Binding to PI(3,4,5)$P_3$ or PI(3,4)$P_2$ results in a conformational change in Akt that relieves a steric block to substrate binding and, together with activation loop and hydrophobic motif phosphorylation, leads to high-affinity substrate binding. Furthermore, disruption of the PH–kinase domain interaction leads to a fourfold increase in the affinity of Akt for PI(3,4,5)$P_3$-containing membranes, indicating that the binding site is at least partially occluded in the inactive conformation. Conformational changes in Akt associated with membrane binding have previously been postulated on the basis of biochemical and cell biological studies (16–21), computational modeling (22, 23), or structures of truncated Akt in complex with inhibitors (24–26), but the exact nature of the conformational change is unknown.

We present here direct biophysical evidence for a large conformational change in Akt associated with membrane binding, and find that a mutant that disrupts the autoinhibitory interactions between the PH and kinase domains mimics these conformational changes. We show that its disruption leads to opening of the kinase and a more extended conformation. We also show, by determining the affinity of the PH–kinase domain interaction, that the inhibitory interface is relatively strong, and serves to maintain cytosolic Akt in a closed conformation 99% of the time at equilibrium. Finally, we present a detailed analysis of the conformational changes that accompany Akt activation by PI(3,4,5)$P_3$ and demonstrate that, in addition to relieving a steric block to substrate binding, the conformational changes govern both Akt activation and inactivation by phosphorylation and dephosphorylation, respectively. Importantly, we show that stoichiometric phosphorylation of Akt does not override PH domain-mediated autoinhibition in the absence of $PIP_3$. In conclusion, we show that Akt is activated by a series of conformational changes beginning with PI(3,4,5)$P_3$ or PI(3,4)$P_2$ binding, and followed by activation loop and hydrophobic motif phosphorylation. Conversely, reversal of those conformational changes upon dissociation from the membrane promotes Akt dephosphorylation and inactivation.

## Results

**Akt Undergoes a Large Conformational Change upon $PIP_3$ Binding.** We previously described a mutation in the kinase domain of Akt1 (Akt1$^{D323A\ D325A}$, referred to hereinafter as Akt1$^{DA}$) that

### Significance

**Akt is a paradigmatic lipid-activated kinase, which is frequently hyperactivated in human cancer. In the absence of PI(3,4,5)$P_3$ or PI(3,4)$P_2$, Akt is maintained in an inactive conformation by an inhibitory interaction between its membrane-binding PH domain and its kinase domain. Here, we describe the conformational changes associated with its binding to PI(3,4,5)$P_3$, leading to disruption of the inhibitory PH–kinase interface, and its consequent activation by protein kinases. Intriguingly, we find that reversal of those conformational changes promotes its inactivation by protein phosphatases. The activation of Akt is thereby restricted to discrete membrane locations, and it is rapidly inactivated upon dissociation. We propose a model in which activation, substrate phosphorylation, and inactivation of Akt are tightly coupled to the membrane.**

Author contributions: I.L. and T.A.L. designed research; I.L., M.K.R., L.T., D.J.H., and T.A.L. performed research; J.E.B. contributed new reagents/analytic tools; I.L., M.K.R., J.E.B., and T.A.L. analyzed data; and T.A.L. wrote the paper.

The authors declare no conflict of interest.

This article is a PNAS Direct Submission. P.N.T. is a guest editor invited by the Editorial Board.



[1]To whom correspondence should be addressed. Email: thomas.leonard@meduniwien.ac.at.

This article contains supporting information online at www.pnas.org/lookup/suppl/doi:10.1073/pnas.1716109115/-/DCSupplemental.

Published online April 9, 2018.

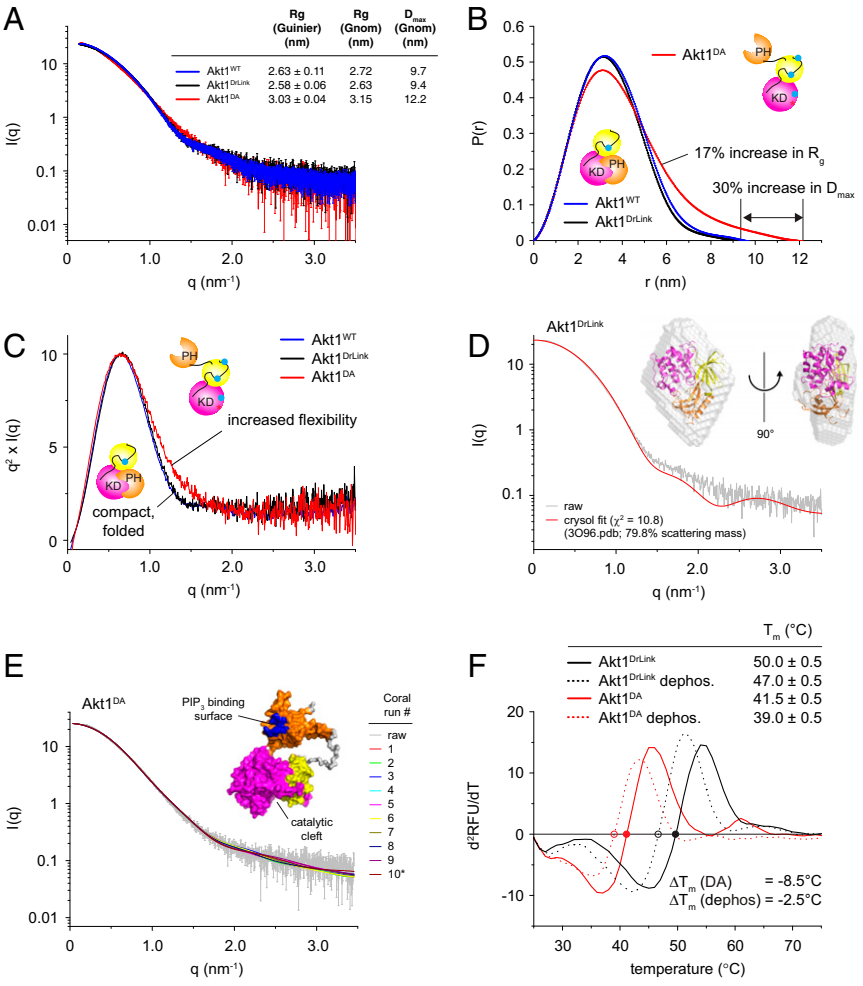


**Fig. 1.** Akt1 undergoes a large conformational change upon PI(3,4,5)P3 binding. (*A*) SAXS curves for Akt1$^{WT}$, Akt1$^{DrLink}$ and Akt1$^{DA}$ in solution. (*Inset*) Table of particle parameters derived from the scattering data. (*B*) Pair distribution functions for Akt1$^{WT}$, Akt1$^{DrLink}$ and Akt1$^{DA}$. (*Inset*) Schematics of Akt conformation: kinase domain (KD; N lobe, yellow; C lobe, magenta), pleckstrin homology domain (PH, orange). (*C*) Kratky plots of Akt1$^{WT}$, Akt1$^{DrLink}$, and Akt1$^{DA}$. Akt1$^{DA}$ exhibits an increase in random coil character compared with Akt1$^{WT}$ and Akt1$^{DrLink}$. (*D*) Fit of crystal structure of Akt1$^{1–443}$ bound to inhibitor VIII (PDB ID code 3O96) to solution scattering of Akt1$^{WT}$. (*Inset*) Fit of 3O96.pdb to the ab initio calculated molecular envelope of Akt1$^{DrLink}$. (*E*) Rigid body modeling of constitutively active Akt1$^{DA}$. The position of the PH domain was fixed, and the kinase domain was allowed to move. Iterative cycles of simulated annealing converged on a model with best fit to the experimental scattering data. Representative models from 10 individual rigid body simulations are compared with the measured scattering curve for Akt1$^{DA}$. (*Inset*) Model from Coral run #10. (*F*) Plot of the second differential of the thermal melting curves of autoinhibited Akt1 (Akt1$^{DrLink}$) and constitutively active Akt1 (Akt1$^{DA}$), as well as their dephosphorylated counterparts (dotted lines), determined by DSF. Melting temperatures ($T_m$) were determined as the temperature at which the second differential is equal to zero (*y* intercepts, indicated with circles).

confers enhanced substrate affinity, enhanced affinity for membrane-embedded $PIP_3$, and resistance to dephosphorylation (12). These observations imply a large conformational change in Akt1 that accompanies $PIP_3$ recognition. To obtain evidence for a conformational change between autoinhibited and membrane-bound Akt1, we used a combination of small-angle X-ray scattering (SAXS), hydrogen–deuterium exchange mass spectrometry (HDX-MS), and in vitro biochemistry.

All Akt1 constructs used in this study are illustrated in *SI Appendix*, Fig. S1. The domain architecture, phosphorylation profile (activation loop, turn motif, and hydrophobic motif), protease cleavage sites, and experimentally validated conformation of each construct are depicted. Recombinant wild-type Akt1 (Akt1$^{WT}$) isolated from baculovirus-infected insect cells is heterogeneously phosphorylated, with five major species isolated by high-resolution anion-exchange chromatography each differing by the mass of a single phosphate (*SI Appendix*, Fig. S2*A*). Tryptic digest mass spectrometry of pentakisphosphorylated Akt1 revealed up to 16 sites of phosphorylation throughout the protein, of which T308 in the activation loop and S473 in the hydrophobic motif are phosphorylated in ∼10% and 0.2% of molecules, respectively (*SI Appendix*, Fig. S2*B*). To generate a chemically monodisperse sample suitable for further structural and biophysical studies, we engineered a mutant protein in which nonconserved, surface-exposed sites phosphorylated on more than 3% of peptides were mutated. As a final step to reduce conformational heterogeneity, we replaced the interdomain linker between the PH and kinase domains with the shortest linker from an alignment of Akt orthologs spanning more than 600 My. The engineered protein, which we call Akt1$^{DrLink}$ (since the linker is derived from the zebrafish *Danio rerio*), is primarily monophosphorylated when isolated from insect cells (*SI Appendix*, Fig. S2 *C* and *D*). Human Akt1 (HsAkt1$^{WT}$), zebrafish Akt1 (DrAkt1$^{WT}$), and our chimeric Akt1$^{DrLink}$ bind PI(3,4)$P_2$ equally in vitro (*SI Appendix*, Fig. S2*E*). Like HsAkt1$^{WT}$, Akt1$^{DrLink}$ is activated similarly by PI(3,4)$P_2$ in vitro (*SI Appendix*, Fig. S2*F*), binds substrate with comparable affinity (*SI Appendix*, Fig. S2*G*), and is phosphorylated on both T308 and S473 in HeLa cells in response to insulin stimulation (*SI Appendix*, Fig. S3*A*). In contrast to Akt1$^{WT}$ and Akt1$^{DrLink}$, recombinant Akt1$^{DA}$ was observed to be hyperphosphorylated (*SI Appendix*, Fig. S3*B*), with ∼57 to 70% of molecules phosphorylated on T308, and 26 to 28% phosphorylated on S473 (*SI Appendix*, Fig. S3*C*).

We next determined the solution structures of Akt1$^{DrLink}$ and Akt1$^{DA}$ by SAXS to characterize the conformational changes associated with disruption of the PH–kinase domain interaction. By applying samples to a size exclusion column in-line with the X-ray beam, we separated out any high molecular weight aggregates in our sample that would distort the subsequent analysis of particle parameters (*SI Appendix*, Fig. S4*A*). The raw scattering curves show a significant difference between the two proteins (Fig. 1*A*), readily appreciated from the calculated pair distribution functions of the two particles (Fig. 1*B*). Akt1$^{DrLink}$ did not exhibit a significant difference from Akt1$^{WT}$, while dephosphorylation of Akt1$^{WT}$ also did not significantly affect the scattering (*SI Appendix*, Fig. S4 *B–D*). In contrast, Akt1$^{DA}$ exhibits a more extended conformation, with a 17% increase in its radius of gyration ($R_g$) and a 30% increase in the maximum dimension ($D_{max}$) of the particle (Fig. 1 *A* and *B* and *SI Appendix*, Fig. S4 *E–H*). The Kratky plot shows that both the engineered (Akt1$^{DrLink}$) and Akt1$^{WT}$ have superimposable

bell-shaped curves, according to Porod's law for globular macromolecules, while constitutively active Akt1 ($Akt1^{DA}$), which mimics the membrane-bound conformation, exhibits an increase in random coil character (Fig. 1*C*). This is presumably due to the loss of interactions between the PH and kinase domains, and the consequent increase in flexibility, caused by the mutation.

We next compared the solution structure of Akt1 with the reported crystal structure of a truncated construct of Akt1 in complex with the allosteric inhibitor, inhibitor VIII (24). While the agreement between the experimental and theoretical scattering curves is not perfect (Fig. 1*D*), 20% of the scattering mass, including important regulatory regions (αC helix, activation loop, C-terminal tail), is missing in the crystal structure. Ab initio calculation of the molecular envelope shows that $Akt1^{DrLink}$ adopts a compact conformation, into which the structure of Akt1 in complex with inhibitor VIII fits reasonably well (Fig. 1*D*, *Inset*).

To evaluate the conformation of $Akt1^{DA}$, we employed rigid body modeling (27) of the PH (residues 1 to 121) and kinase (residues 144 to 477) domains of Akt1 [Protein Data Bank (PDB) ID code 1UNP (28) and PDB ID code 4EKK (29), respectively] with an interdomain linker of 23 amino acids. The PH domain position was fixed and the kinase domain allowed to move according to the restraints imposed by the linker. Iterative cycles of rigid body modeling converged on a set of models in which Akt1 adopts a more compact than expected conformation, but with both the $PIP_3$-binding surface of the PH domain and the substrate binding cleft of the kinase domain always solvent-exposed (Fig. 1*E* and *SI Appendix*, Fig. S5*A*).

Finally, we sought to evaluate the stability of the PH–kinase domain interface by comparing the thermal stability of $Akt1^{DrLink}$ with that of $Akt1^{DA}$. $Akt1^{DA}$ is destabilized by 8.5 °C with respect to $Akt1^{DrLink}$ (Fig. 1*F*), indicating that the PH–kinase interface considerably stabilizes the full-length protein. Dephosphorylation of both proteins (*SI Appendix*, Fig. S5 *B* and *C*) reduced their thermal stabilities by a further 2.5 °C to 3 °C (Fig. 1*F*), most likely by removing the constitutive stabilizing phosphorylation of T450 in the turn motif.

**Steady-State Autoinhibition of Akt by PH Domain Sequestration.** We previously observed that disruption of the PH–kinase domain interface not only rendered Akt1 insensitive to $PIP_3$, but also enhanced its binding to $PIP_3$-containing liposomes and its accumulation at the plasma membrane in response to growth factor stimulation (12). These observations imply that the $PIP_3$-binding site is at least partially occluded in the autoinhibited conformation of Akt. Having also observed that a model substrate peptide could bind to autoinhibited Akt1, albeit at very low affinity, we concluded that inactive Akt most likely exists in an equilibrium of open and closed conformers.

To determine the position of the intramolecular equilibrium, and thereby estimate the degree of autoinhibition in the cytosol of unstimulated cells, we measured the affinity of the isolated purified kinase domain for the isolated PH domain by fluorescence anisotropy. Mass spectrometry showed the purified kinase domain to be exclusively monophosphorylated (*SI Appendix*, Fig. S6 *A* and *B*), predominantly in the turn motif (T450) as judged by Western blotting with phosphospecific antibodies (*SI Appendix*, Fig. S6*C*). Fitting of the data with a one-site binding model gave an equilibrium dissociation constant, $K_d$, of 7 μM (Fig. 2*A*), which corresponds to a fraction of the closed, PH domain bound, conformer equal to 98.8% at equilibrium (Fig. 2*B*). This is further increased to 99.9% if one assumes a more compact interdomain linker (*SI Appendix*, Fig. S5*A*) rather than the maximum contour length of a 23-amino acid peptide.

Activation of Akt by $PIP_3$ or $PI(3,4)P_2$ suggests that Akt activity is confined to the membrane environment, an observation corroborated by our previous findings in vivo, which showed that active Akt exhibits diffusion properties consistent with a membrane-bound species (12). However, the soluble polyphosphate inositol-1,3,4,5-tetrakisphosphate ($IP_4$) has also been recognized as an important second messenger in cells (30–32), so, to rule out the possibility that $IP_4$ could activate Akt in the cytosol, we assayed the ability of $IP_4$ to competitively displace the kinase domain of Akt from Atto488-labeled PH domain. Consistent with the requirement for membrane-embedded $PIP_3$ or $PI(3,4)P_2$, we observed that $IP_4$ was unable to displace the kinase domain at concentrations up to 330 μM (Fig. 2*C*) or activate Akt1 in an in vitro kinase assay under conditions in which Akt1 is activated by an equimolar concentration of $PIP_3$ (Fig. 2*D*).

**$PIP_3$ Engagement Drives Conformational Changes Required for Activation.** Having established that Akt1 undergoes a large conformational change upon disruption of the PH–kinase domain interface, we sought to map the conformational changes associated with both $PIP_3$ binding and Akt phosphorylation in more detail using HDX-MS. HDX-MS is an analytical technique that measures the exchange rate of amide hydrogens with solvent, and, as the main determinant of amide exchange is involvement in secondary structure, it can be used as a readout of protein conformational dynamics (33). It has been used as a powerful tool to examine protein conformational changes that occur upon membrane recruitment (34–36).

To evaluate the effect of both $PIP_3$ binding and the mutation in $Akt1^{DA}$, we compared HDX in $Akt1^{DrLink}$ and $Akt1^{DA}$ both in solution and bound to $PIP_3$-containing liposomes. We used chemically monodisperse $Akt1^{DrLink}$ in place of $Akt1^{WT}$ for this analysis, as it allowed us to examine the protein conformations of the maximally inhibited form of Akt1 ($Akt1^{DrLink}$) compared with the hyperactivated form ($Akt1^{DA}$). All HDX peptide data for $Akt1^{DrLink}$ and $Akt1^{DA}$, in the presence and absence of $PIP_3$-containing vesicles, can be found in *SI Appendix*, Figs. S7 and S8 respectively.

We observed significant changes in the rates of H/D exchange in a number of peptides corresponding to both the PH and kinase domains (*SI Appendix*, Fig. S9) that occurred upon membrane binding, and between the activated and inactivated forms in solution. There were no differences in exchange in $Akt1^{DrLink}$ when exposed to liposomes lacking $PI(3,4,5)P_3$ (*SI Appendix*, Fig. S10), verifying that conformational changes were not due to a nonspecific membrane effect. To determine the conformational changes that occurred upon binding of the inhibited form of Akt1 ($Akt1^{DrLink}$) to $PIP_3$-containing membranes, we examined the differences in the rates of H/D exchange between free (unbound) and $PIP_3$-bound Akt1 (Fig. 3*A*). By comparing these changes to those observed in the activated form of $Akt1^{DA}$ bound to membranes, we could separate conformational changes driven by membrane interaction of the PH domain, compared with those mediated by disruption of the PH–kinase domain interface. We observed, in both proteins, that the rate of exchange is dramatically lower over the entire PH domain in the presence of $PIP_3$ vesicles, consistent with its protection upon binding (Fig. 3 *A* and *B*). Larger decreases in exchange in the PH domain of $Akt1^{DA}$ compared with $Akt1^{Drlink}$ are most likely reflected in the competition between the kinase domain and $PIP_3$ for the PH domain in $Akt1^{DrLink}$ (and the consequent enhanced affinity of $Akt1^{DA}$ for $PIP_3$) such that, under the same conditions, $Akt1^{DA}$ is more tightly bound to the membrane (12) and therefore exhibits greater protection of its PH domain.

$PIP_3$ binding also resulted in a dramatic deprotection of residues in the kinase domain of $Akt1^{DrLink}$ encompassing the activation loop and helix αG in the C lobe, consistent with this surface of the C lobe being the major surface of interaction with the PH domain. $Akt1^{DA}$ showed much smaller increases in exchange upon $PIP_3$ binding, consistent with the mutation destabilizing this interface. These observations indicate that the nonphosphorylated activation loop is sequestered in the autoinhibited state of Akt, consistent with biochemical studies showing that $PIP_3$ binding enhances phosphoinositide-dependent kinase 1 (PDK1)-dependent activation loop phosphorylation (16, 17).

Curiously, increases in exchange are also seen upon membrane binding in residues 218 to 225 in strands β4 and β5 of the N lobe, but only in $Akt1^{DrLink}$. Strands β4 and β5, together with helices αB and

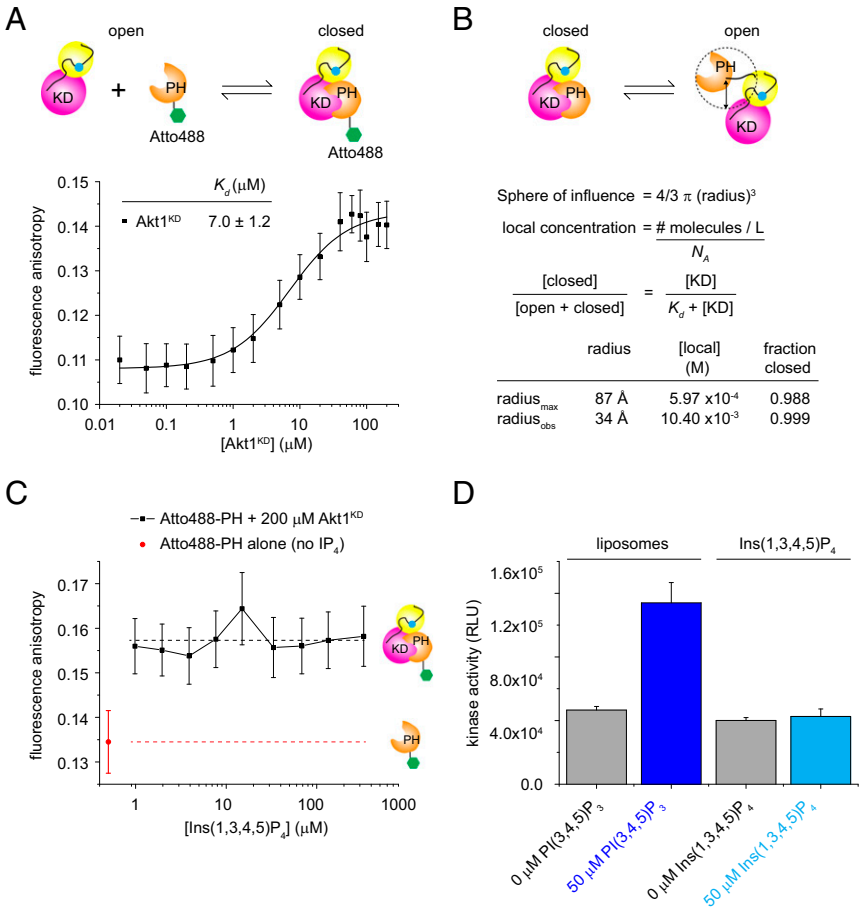


**Fig. 2.** Steady-state autoinhibition of Akt by PH domain sequestration. (*A*) Determination of the affinity of the kinase domain for the PH domain of Akt1 by fluorescence anisotropy. Akt1$^{1–120}$ T101C was labeled in vitro with Atto488 (see *Materials and Methods*); 100 nM Atto488-labeled PH domain was incubated with 220 μM Akt1$^{KD}$. The binding curve was constructed by making serial dilutions in buffer containing 100 nM Atto488-labeled PH domain. Error bars are the SD of 50 measurements from three independent experiments. (*B*) Calculation of the position of equilibrium between open and closed states of Akt1 using a sphere of influence to estimate the local concentration of the two domains with respect to each other. (*C*) Competitive displacement of kinase domain from PH domain with $IP_4$, measured by fluorescence anisotropy; 100 nM Atto488-labeled PH domain was incubated with 280 μM unlabeled kinase domain to form a PH:KD complex (black dashed line). $IP_4$ does not result in dissociation of the PH domain (red dashed line) at concentrations up to 330 μM. Error bars are the SD of 50 independent measurements. (*D*) In vitro kinase assay of Akt in the presence of $PIP_3$-containing liposomes or soluble Ins(1,3,4,5)$P_4$. Error bars are the SD of triplicate measurements.

αC, form the hydrophobic pocket on the N lobe of the kinase domain that accommodates the hydrophobic motif in the C-terminal tail of Akt. Q218 makes a hydrogen bond to phospho-S473 in the active conformation, thereby stabilizing the hydrophobic motif and the conformation of the αC helix (37), but the conformation of the hydrophobic motif in the absence of phosphorylation is unknown. Deprotection of strands β4 and β5 suggests an exposure of this region upon $PIP_3$ binding that may release the unphosphorylated C-terminal tail for phosphorylation, although it should be noted that we did not observe a corresponding change in the H/D exchange rates in the C terminus. Conversely, in Akt1$^{DA}$, in which the PH domain has been disengaged from the kinase domain in the absence of membrane binding and the kinase domain is hyperphosphorylated on T308 and S473 (12), strands β4 and β5 exhibit much lower rates of H/D exchange that are unchanged by $PIP_3$ binding. This is consistent with a disorder-to-order transition of the hydrophobic motif mediated by S473 phosphorylation, previously observed in crystal structures of the isolated kinase domain in the absence of phosphorylation and in the presence of a phosphomimetic at this position (37).

Since it has been previously proposed that phosphorylation could render Akt active in the absence of $PIP_3$ (18, 20, 38, 39), we next sought to separate out conformational changes elicited by phosphorylation from those elicited by $PIP_3$ binding. We first compared the conformation of dephosphorylated Akt1$^{DrLink}$ with dephosphorylated Akt1$^{DA}$ free in solution by HDX-MS. This comparison allowed us to look at conformational changes solely caused by disruption of the PH–kinase interface, with no interference from different phosphorylation states. Compared with dephosphorylated Akt1$^{DrLink}$, dephosphorylated Akt1$^{DA}$ exhibits deprotection of both the kinase domain C lobe and the PH domain, consistent with exposure of the $PIP_3$ binding site, activation loop, and catalytic cleft (Fig. 3*C*) and replicating the deprotection of the kinase domain exhibited by Akt1$^{DrLink}$ when bound to $PIP_3$ liposomes (Fig. 3*A*). This observation unambiguously rules out hyperphosphorylation of Akt1$^{DA}$ as the mediator of the conformational changes.

To rule out that stoichiometric phosphorylation of Akt could drive the observed conformational changes in the absence of $PIP_3$, we phosphorylated Akt1$^{DrLink}$ S473D with PDK1 in vitro (*SI Appendix*, Fig. S11*A*) to generate Akt1$^{DrLink}$ pT308 S473D, a construct designed to mimic Akt phosphorylated on all three sites (T308, T450, and S473). Akt1$^{DrLink}$ pT308 S473D was confirmed to be >90% diphosphorylated (*SI Appendix*, Fig. S11*B*) on T308 (activation loop) and T450 (turn motif) (*SI Appendix*, Fig. S11*C*). We next compared the conformation of stoichiometrically phosphorylated Akt1$^{DrLink}$ S473D to dephosphorylated Akt1$^{DrLink}$ free in solution by HDX-MS. All HDX peptide data for Akt1$^{DrLink}$ pT308 S473D, Akt1$^{DrLink}$ dephosphorylated (dephos.), and Akt1$^{DA}$ dephos. can be found in *SI Appendix*, Fig. S12. Peptides exhibiting significant changes in H/D exchange are plotted in *SI Appendix*, Fig. S13.

The PH domain exhibits no significant changes in H/D exchange, indicating that the PH–kinase autoinhibitory interface is maintained even when Akt1 is constitutively phosphorylated (Fig. 3*D*). This is further supported by thermal stability measurements, which indicate that stoichiometric phosphorylation does not affect the thermal stability of Akt1 (Fig. 3*E*). The N and C lobes of the kinase domain exhibit protection and deprotection, respectively, in the phosphorylated protein (Fig. 3*D*). The deprotection of the kinase C lobe and, in particular, the activation loop is consistent with the failure of the phosphorylated activation loop to adopt a sequestered conformation in the autoinhibited conformation of Akt (Fig. 3*A*). The protection of peptides in the N lobe of Akt1$^{DrLink}$ pT308 S473D most likely arises from the phosphorylation of the turn motif (T450), a constitutive site known to stabilize Akt (11). When phosphorylated, T450 is coordinated by

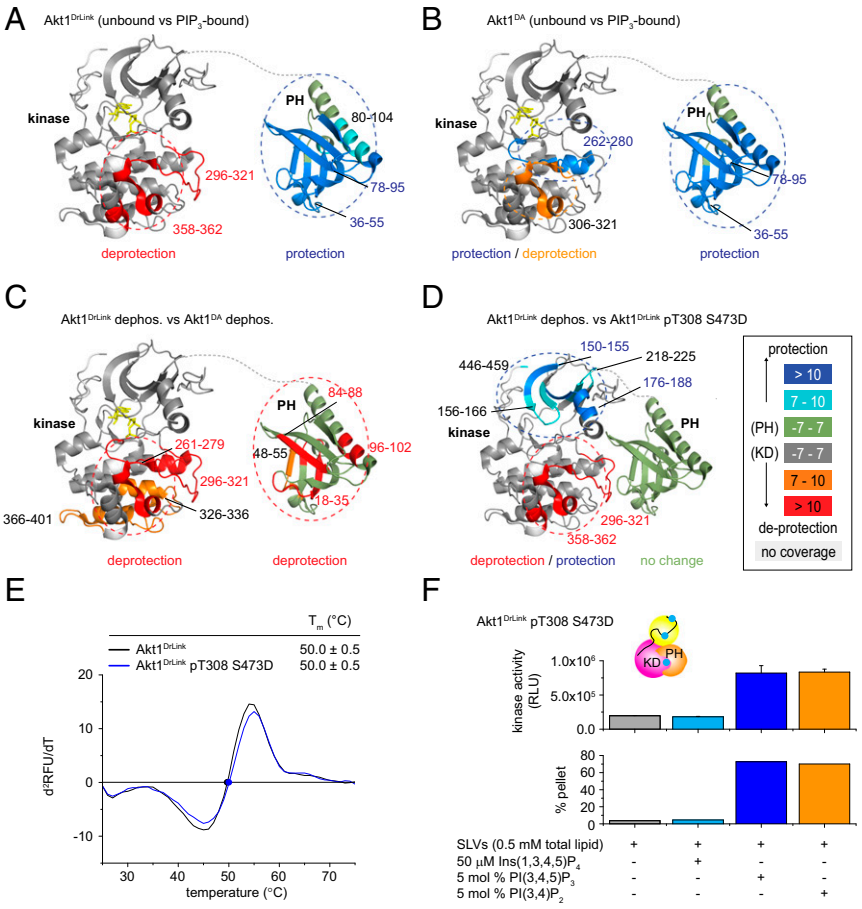


**Fig. 3.** PI(3,4,5)$P_3$ engagement drives conformational changes required for activation. (*A*) Changes in hydrogen–deuterium exchange between Akt1$^{DrLink}$ in solution (unbound) and in the presence of $PIP_3$-containing liposomes (bound) mapped onto the structures of the Akt1 PH and kinase domains (PDB ID codes 4ekk and 1unq). For all panels, peptides that showed significant differences in exchange at any time point (greater than both a 7% difference in % deuterium incorporation and a 0.4-Da difference in deuterium incorporation with a Student *t* test value of <0.01) were mapped on to the structure. In the models, the active site is indicated by bound nucleotide shown in yellow. (*B*) Changes in hydrogen–deuterium exchange between Akt1$^{DA}$ in solution (unbound) and in the presence of $PIP_3$-containing liposomes (bound) mapped onto the structures of the Akt1 PH and kinase domains. (*C*) Changes in hydrogen–deuterium exchange between dephosphorylated Akt1$^{DrLink}$ and dephosphorylated Akt1$^{DA}$ in solution mapped onto the structures of the Akt1 PH and kinase domains. (*D*) Changes in hydrogen–deuterium exchange between dephosphorylated Akt1$^{DrLink}$ and stoichiometrically phosphorylated Akt1$^{DrLink}$ pT308 S473D in solution mapped onto the structures of the Akt1 PH and kinase domains. (*E*) Thermal stability of Akt1$^{DrLink}$ pT308 S473D compared with Akt1DrLink (monophosphorylated on T450). Phosphorylation of T308 and S473 does not affect the thermal stability of Akt1. (*F*) In vitro kinase assay for Akt1$^{DrLink}$ pT308 S473D using Crosstide substrate and liposomes containing either 0 mol % or 5 mol % PI(3,4,5)$P_3$, PI(3,4)$P_2$, or 50 μM Ins(1,3,4,5)$P_4$.

a basic patch of residues on the N lobe comprising K158, K163, K182, and R222, all of which are found in the protected peptides.

Having established that phosphorylation does not result in major conformational changes in Akt1 in the absence of $PIP_3$, we tested the hypothesis that the kinase activity of phosphorylated Akt1 should be $PIP_3$-dependent. As expected, phosphorylation fails to override the activation by both PI(3,4,5)$P_3$ and PI(3,4)$P_2$ (Fig. 3*F* and *SI Appendix*, Fig. S14), consistent with the formation of the autoinhibited conformation in the absence of membrane binding, irrespective of phosphorylation.

In summary, Akt1 adopts a compact, autoinhibited conformation in the absence of $PIP_3$ irrespective of its phosphorylation state. In solution, the substrate binding cleft, including the activation loop and catalytic loop, is sequestered in an inactive conformation, while the $PIP_3$-binding pocket is at least partially occluded in the interface. Upon membrane binding, the PH domain, activation loop, and possibly also the C-terminal tail are displaced from the kinase domain, priming Akt for phosphorylation and substrate binding. Upon dissociation from $PIP_3$, Akt adopts an autoinhibited conformation, displacing the phosphorylated activation loop from its active conformation and priming it for dephosphorylation.

**Membrane and ATP Binding Cooperatively Protect Akt from Dephosphorylation.** We previously showed that Akt is more rapidly dephosphorylated in vivo in the presence of its PH domain (12), while other studies have demonstrated a role for ATP in stabilizing the phosphorylated, active conformation (29, 40, 41). Having observed that, in the absence of $PIP_3$, Akt adopts an autoinhibited conformation in which the phosphorylated activation loop is exposed (Fig. 3*D*), we hypothesized that ATP-dependent caging of the regulatory phosphates could only be possible in the context of membrane binding, since the PH domain occludes the docking surface on the kinase domain for the phosphorylated activation loop. To establish whether phosphorylated Akt is stabilized by ATP in the context of membrane binding, but efficiently dephosphorylated in solution, we evaluated the dephosphorylation kinetics at T308 and S473 under conditions mimicking membrane binding (Akt1$^{DA}$ or isolated kinase domain) or free in solution, in the presence and absence of ATP.

The active conformation of the isolated kinase domain of Akt exhibits a network of interactions between the N and C lobes of the kinase domain, stabilized by ATP, and both the phosphorylated activation loop (T308) and hydrophobic motif (S473) (41, 42). We first established that phosphorylation of these two residues leads to an almost fourfold higher affinity for ATP by comparing the constitutively active Akt1$^{DA}$ (hyperphosphorylated on T308 and S473) to the kinase domain alone (monophosphorylated on T450) (*SI Appendix*, Fig. S15).

To test whether ATP-dependent caging of pT308 is context-dependent, we took advantage of 3C-cleavable Akt1$^{3C}$ (*SI Appendix*, Fig. S1) that contained a phosphomimetic amino acid at S473 (S473D). We previously showed that this mutation does not override the dependency on $PIP_3$ for Akt activation (12). We generated free kinase domain (Akt1$^{KD}$ S473D) from autoinhibited Akt1$^{3C}$ S473D by cleaving the full-length protein with 3C protease and separating the kinase and PH domains by size exclusion chromatography. Removal of the PH domain in this way mimics the relief of autoinhibition upon membrane binding. Both proteins were then treated with lambda phosphatase in the absence and presence of ATP (Fig. 4*A*). This approach has two clear advantages: (*i*) The stoichiometry of T308 phosphorylation is equal in both proteins and (*ii*) the dephosphorylation kinetics can be compared in the same reaction, since the two proteins can be resolved on a Western blot. While the isolated kinase domain shows a small but statistically significant degree of protection from T308

dephosphorylation in the absence of ATP (Fig. 4*B*), it is dramatically protected from dephosphorylation in the presence of ATP compared with full-length, autoinhibited Akt1 (Fig. 4*C*). The protection of pT308 in the absence of ATP likely arises from a lower-affinity interaction between the activation loop and the C lobe of the kinase domain even in the absence of ATP. Curiously, in the presence of ATP, both curves can be fit to a monoexponential decay with the same time constant, but, while full-length Akt1 is almost completely dephosphorylated in the course of the assay, the kinase domain is only ~20% dephosphorylated. This suggests that a fraction of the kinase domain cannot be protected by ATP, perhaps due to substoichiometric turn motif phosphorylation.

We next compared the dephosphorylation kinetics of hyperphosphorylated $Akt1^{DA}$, which has a disrupted PH–kinase interface, with those of $Akt1^{3C}$ S473D (Fig. 4*D*). Like the isolated kinase domain, $Akt1^{DA}$ exhibited identical dephosphorylation kinetics to $Akt1^{3C}$ S473D in the absence of nucleotide (Fig. 4*E*), but, in the presence of ATP, $Akt1^{3C}$ S473D was dephosphorylated on T308 significantly faster than $Akt1^{DA}$ (Fig. 4*F*), indicating that interaction of the PH and kinase domains renders the activation loop more accessible for dephosphorylation. While the isolated kinase domain is robustly protected by ATP (Fig. 4*C*), $Akt1^{DA}$ is completely dephosphorylated, albeit with slower kinetics than $Akt1^{3C}$ S473D. This is likely due to residual interactions between the kinase and PH domains of $Akt1^{DA}$ (Fig. 3*B*) that destabilize the phosphorylated activation loop even in the presence of ATP.

Finally, we investigated the stability of the phosphorylated hydrophobic motif in the context of membrane binding. To demonstrate that this is an intrinsic property of Akt, we incubated $Akt1^{WT}$ with liposomes containing 0 mol % or 5 mol % $PIP_3$ in the presence or absence of ATP (Fig. 4*G*). We observed that Akt1 is significantly protected from hydrophobic motif dephosphorylation in the presence of $PIP_3$-containing liposomes (Fig. 4*H*) and that this is further enhanced by ATP binding (Fig. 4*I*). It should be noted that a technical limitation of this experiment is the requirement to keep magnesium concentrations low enough to support $PIP_3$ binding (12). Given the affinity for ATP (~100 μM), only 50% of Akt1 will be ATP-bound under these experimental conditions (100 μM ATP, 200 μM $MgCl_2$), and therefore the protection of the hydrophobic motif by ATP and $PIP_3$ is significantly underestimated.

In conclusion, Akt is protected from dephosphorylation in an ATP- and $PIP_3$-dependent manner. While $PIP_3$-bound, Akt is protected from dephosphorylation by ATP-dependent caging of its regulatory phosphates, but, upon dissociation, Akt is rapidly dephosphorylated and inactivated.

## Discussion

Protein kinases transfer phosphate from ATP to an acceptor serine, threonine, or tyrosine residue in a protein chain. While some specificity may be achieved by recognition of the primary acceptor sequence, the stereochemistry of phosphotransfer is essentially the same for the more than 500 human protein kinases (43). Therefore, in order for the cell to perform the myriad signaling reactions transduced by protein kinases, it must regulate their activity, both spatially and temporally, within the cell. Various mechanisms of protein kinase regulation have been described, including activation loop phosphorylation, steric occlusion of the catalytic cleft, requirement for accessory proteins, autoinhibition by regulatory domains, complex formation by scaffolding proteins, and spatial segregation of kinase and substrate (44–48).

The protein kinase Akt phosphorylates substrates involved in growth, survival, differentiation, and metabolism, with over 100 reported substrates (1). Despite the fact that not all substrates have been carefully validated, the evidence points to a context-dependent phosphorylation of a diverse array of downstream effectors by Akt, necessitating its tight regulation. Akt activity depends strictly on activation by PDK1 and mechanistic target of rapamycin complex 2 (mTORC2) at the plasma membrane, following growth factor stimulation. The localization of substrates in subcellular compartments distal to the plasma membrane, however, led to the proposal that Akt could dissociate from the membrane, locked in an active conformation (17, 18, 20, 38, 39). By diffusion, Akt would encounter its substrates within the cell, and its activity would be controlled by the rate at which phosphatases inactivated it (38, 39). This model, however, proposes a scenario in which Akt activity is uncoupled from its activating stimulus, as well as spatially delocalized in the cell, which would serve to diminish, rather than enhance, substrate specificity.

We recently demonstrated that the activity of Akt is strictly confined to membranes containing either $PIP_3$ or $PI(3,4)P_2$. $PI(3,4,5)P_3$ and $PI(3,4)P_2$ allosterically activate Akt by relieving steric occlusion of the substrate binding cleft (12). While previous studies failed to observe the direct activation of Akt by $PI(3,4,5)P_3$ (9, 16), the reported kinase assays were performed under conditions of high magnesium (5 mM to 10 mM), which significantly attenuates Akt binding to $PI(3,4,5)P_3$ (12) and, hence, its activation. This has likely obscured the observation of direct activation of Akt by $PIP_3$ in previous studies.

We now show that autoinhibited Akt forms a compact structure in which the PH and kinase domains are held together by a relatively tight intramolecular interaction that sequesters the $PIP_3$ binding site in the interface. The strength of the interaction coupled with the high local concentration of the kinase and PH domains with respect to each other serves to maintain Akt in a closed conformation inaccessible to substrate more than 99% of the time at equilibrium. Presumably, the small fraction (~0.1 to 1.0%) of Akt in the open conformation at equilibrium is sufficient to sense and respond to $PIP_3$, which essentially shifts the equilibrium to the open, membrane-bound conformation. The soluble polyphosphate inositol $IP_4$ is unable to displace this inhibitory interaction or activate Akt at a concentration 100 times that reported in cells (49), reinforcing the absolute requirement for binding to $PIP_3$ or $PI(3,4)P_2$. The inability of $IP_4$ to activate Akt is consistent with previous observations that the active conformation of Akt in cells is associated with a membrane compartment (12), while a separate study has also implicated the bulk phospholipid phosphatidylserine in promoting $PIP_3$ binding and Akt activation (50).

Mutation of two surface-exposed aspartates on the kinase domain led to $PIP_3$-independent Akt activity, Akt hyperphosphorylation, and high-affinity substrate binding independent of membrane binding (12). Implicit from this work was a large conformational change that accompanies Akt activation, which we have now observed directly in solution. The extended conformation of $Akt1^{DA}$ in solution is consistent with disruption of the PH–kinase interface, which exerts a strong stabilizing effect over the entire $Akt1^{WT}$ molecule as indicated by the reduced thermal stability of $Akt1^{DA}$.

HDX-MS allowed us to map experimentally the conformational changes that accompany Akt binding to membrane localized $PIP_3$. The surfaces of interaction identified are consistent with cross-linking mass spectrometry (19) and the relative positions of the PH and kinase domains observed in the structure of Akt1 bound to the allosteric inhibitor VIII (24). We now show, however, that the PH domain interacts not only with the C lobe of the kinase domain surrounding D323 and D325 but also with the unphosphorylated activation loop. The deprotection of the activation loop upon $PIP_3$ binding is consistent with previously reported biochemistry that showed a dependency on $PIP_3$ binding for PDK1 phosphorylation (16, 17). Interestingly, deprotection is also seen for the region of the N lobe that forms the hydrophobic pocket into which the hydrophobic motif of the C-terminal tail binds following its phosphorylation (37). This observation suggests that the unphosphorylated hydrophobic motif likely docks to the same pocket in the autoinhibited conformation of Akt, thereby restricting the availability of the C tail to mTORC2. The docking of the C tail to the hydrophobic pocket in the inactive state was previously proposed (23) but lacked direct evidence, while deletion of the PH domain of Akt was also observed to promote hydrophobic motif phosphorylation in the absence of mTORC2 (51). In summary, both the activation loop

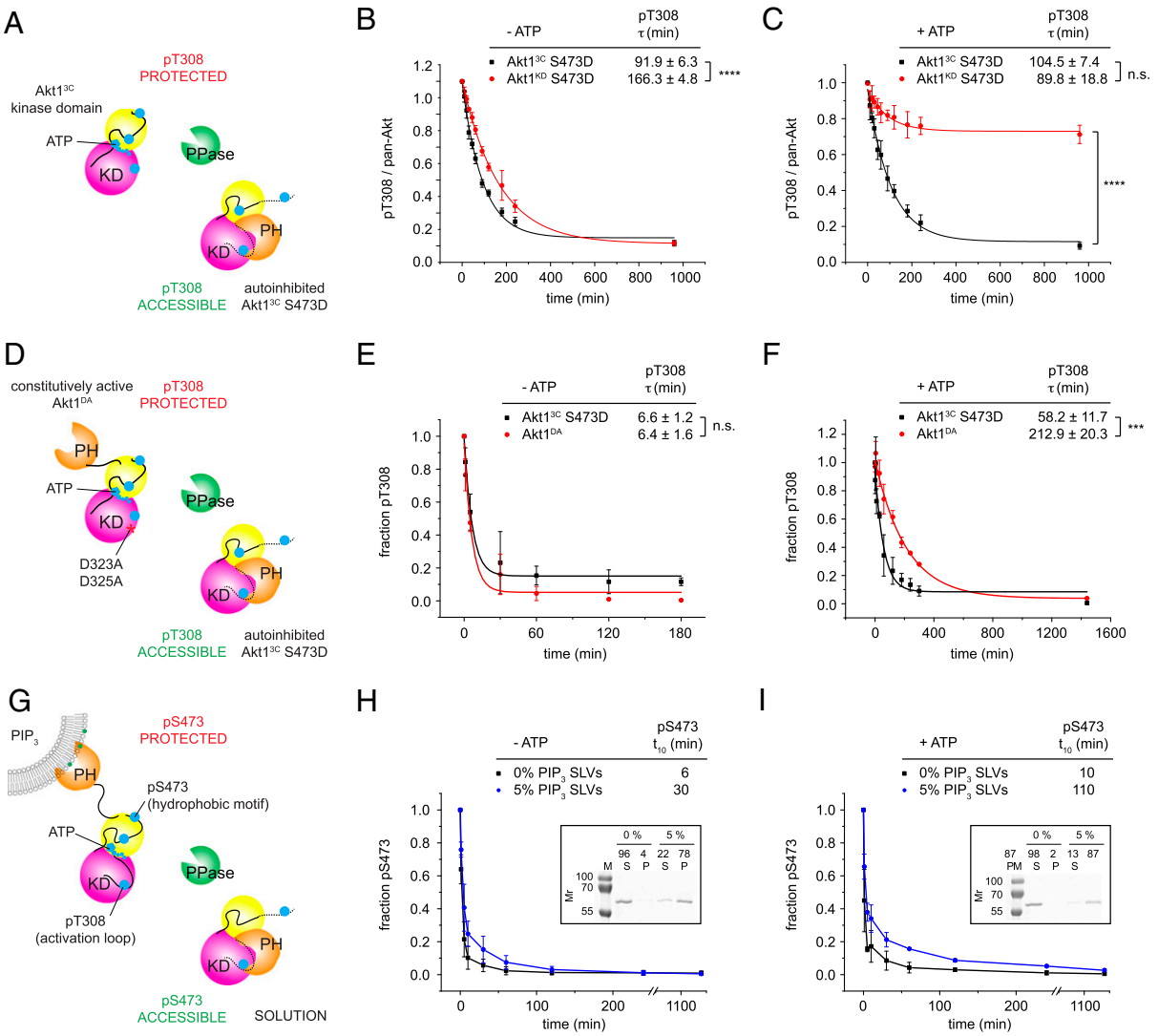


**Fig. 4.** Membrane and ATP binding cooperatively protect Akt from dephosphorylation. (*A*) Cartoon schematic of dephosphorylation assay reported in *B* and *C*. Full-length Akt1$^{3C}$ S473D and its isolated kinase domain were treated with lambda phosphatase in the absence and presence of ATP, and the kinetics of dephosphorylation were measured by quantitative Western blotting. (*B*) Dephosphorylation kinetics of autoinhibited Akt1 (Akt1$^{3C}$ S473D) and its liberated kinase domain (Akt1$^{KD}$ S473D) in the absence of ATP. Error bars are the SD of three independent experiments. Note that, due to variable lambda phosphatase activity, the comparisons of time constants and asymptotes between Akt1 proteins is only valid within individual experiments that were conducted simultaneously with the same batch of phosphatase (represented by a single panel). (*C*) Dephosphorylation kinetics of autoinhibited Akt1 (Akt1$^{3C}$ S473D) and its liberated kinase domain (Akt1$^{KD}$ S473D) in the presence of ATP. Error bars are the SD of three independent experiments. The data in *B* and *C* were fit to monoexponential decay functions and the statistical significance of the difference between the offsets was evaluated with an *F* test (n.s., not significant; ****$P < 0.0001$). (*D*) Cartoon schematic of dephosphorylation assay reported in *E* and *F*. Akt1$^{3C}$ S473D and Akt1$^{DA}$ were treated with lambda phosphatase in the absence and presence of ATP. (*E*) Dephosphorylation kinetics of autoinhibited Akt1 (Akt1$^{3C}$ S473D) and constitutively active Akt1 (Akt1$^{DA}$) in the absence of ATP. (*F*) Dephosphorylation kinetics of autoinhibited Akt1 (Akt1$^{3C}$ S473D) and constitutively active Akt1 (Akt1$^{DA}$) in the presence of ATP. Error bars are the SD of two independent experiments. The data in *E* and *F* were fit to monoexponential decay functions and the statistical significance of the difference between the estimated time constants was evaluated with an *F* test (n.s., not significant; ***$P < 0.001$). (*G*) Cartoon schematic of dephosphorylation assay reported in *H* and *I*. Akt1$^{WT}$ was incubated with liposomes ±PIP$_3$ and treated with lambda phosphatase in the absence and presence of ATP. (*H*) Dephosphorylation kinetics of Akt1$^{WT}$ in the presence and absence of PIP$_3$-containing liposomes, in the absence of ATP. Recombinant Akt1 was incubated with liposomes containing 0 mol % or 5 mol % PIP$_3$ for 30 min before the addition of lambda phosphatase. Error bars are the SD of two independent experiments. (*Inset*) The fraction of Akt bound to liposomes containing either 0 or 5 mol % PIP$_3$ was determined by liposome pelleting. (*I*) Dephosphorylation kinetics of Akt1$^{WT}$ in the presence and absence of PIP$_3$-containing liposomes, in buffer containing ATP. Error bars are the SD of two independent experiments. Due to the convolution of multiple equilibria in *H* and *I* (membrane binding, ATP binding) and nonsaturating ATP concentrations, these data were not subjected to curve fitting. (*Inset*) The fraction of Akt bound to liposomes containing either 0 or 5 mol % PIP$_3$ was determined by liposome pelleting.

and hydrophobic motif are sequestered in the autoinhibited conformation of Akt, requiring PIP$_3$ binding to drive their displacement and consequent accessibility for phosphorylation.

While it has been previously proposed that phosphorylation of Akt could lock it in an active conformation able to dissociate from the plasma membrane and phosphorylate substrates elsewhere in the cell (18, 20, 38), we observe that Akt adopts an autoinhibited conformation even when stoichiometrically phosphorylated. Notwithstanding the fact that this conformation blocks substrate binding, we also observed that Akt is efficiently dephosphorylated in the absence of membrane binding. Although our observations reinforce the ATP-dependent caging of pT308 and pS473 (29, 40,

41), we show that $PIP_3$ binding cooperates with ATP in protecting Akt from dephosphorylation. Dissociation from $PIP_3$ therefore not only results in PH domain-mediated autoinhibition, but also drives Akt inactivation by promoting its dephosphorylation. While not explicitly addressed, this context dependency was hinted at in a previous study in which the ATP-dependent caging of pT308 in full-length Akt1 was observed using immunoprecipitated myristoylated Akt1 incubated with lipids (40). It is therefore likely that the authors were in fact observing the ATP-dependent protection of pT308 in the context of activated, membrane-bound Akt1. Along the same lines, the paradoxical hyperphosphorylation of Akt caused by ATP-competitive Akt inhibitors (52, 53) may be a direct consequence of the inhibitor interfering with reformation of the autoinhibited conformation. Indeed, this is supported by the potentiation of membrane binding elicited by inhibitors and the requirement for a conformational change in addition to membrane localization to drive hyperphosphorylation (52). While hyperphosphorylated Akt isolated from inhibitor-treated cells was observed to be more active, increased substrate phosphorylation in vivo was not observed, consistent with the rapid dephosphorylation of Akt upon inhibitor removal. Concerns about Akt inhibitor-induced pathway activation in cancer patients are therefore likely unfounded.

In summary, Akt is activated by a series of ordered conformational changes and phosphorylation events that accompany $PIP_3$ binding (Fig. 5). In the cytosol, Akt adopts a predominantly compact, inactive conformation in which the PH domain blocks the substrate binding cleft and the regulatory phosphorylation sites of the activation loop and hydrophobic motif are sequestered from activating kinases by intramolecular interactions. A small fraction of Akt adopts an open conformation at equilibrium, which exposes the $PIP_3$ binding pocket of the PH domain, thereby allowing Akt to sense $PIP_3$ in the membrane. Binding shifts the equilibrium to a membrane-bound, extended conformation in which the catalytic cleft is unblocked and the regulatory sites of the kinase domain are exposed to PDK1 and mTORC2. Phosphorylation of these sites results in structuring of the catalytic cleft (activation loop) and organization of the catalytic residues (hydrophobic motif) for phosphotransfer. Conversely, upon attenuation of the $PIP_3$ signal by lipid phosphatases such as phosphatase and tensin homolog (PTEN), Akt dissociates from the membrane, the conformational changes are reversed, and this leads to an exposure of the phosphorylated activation loop and hydrophobic motif to phosphatases. Dephosphorylation of the hydrophobic motif by PH domain leucine-rich repeat-containing protein phosphatase (PHLPP) (54) and the activation loop by PP2A (55, 56) returns the kinase to the autoinhibited state in which the unphosphorylated regulatory sites are sequestered in an inaccessible conformation. In conclusion, Akt activation, substrate phosphorylation, and inactivation are all tightly coupled to the membrane ligands $PI(3,4,5)P_3$ and $PI(3,4)P_2$, thereby restricting Akt activity to membrane sites enriched in these signaling lipids.

Future work to address the atomic details of each step in the mechanism will require a structure of full-length Akt in the physiologically relevant inactive conformation. Structures of Akt1 in complex with allosteric inhibitors have relied on deletion of the C-terminal tail and exhibit a disordered activation loop and αC helix, important regulatory regions that are sequestered/ordered in the inactive conformation. Nevertheless, these structures are entirely consistent with the activation of Akt by mutation of the PH–kinase interface.

## Materials and Methods

**SAXS.** SAXS data were collected on Akt1 proteins using an in-line size exclusion chromatography setup on BM29 at the European Synchrotron Radiation Facility (ESRF). Proteins were applied to a Superdex 200 column equilibrated in 20 mM Tris, pH 7.4, 100 mM NaCl, and 1 mM Tris carboxyethyl phosphine (TCEP), and images were acquired every second for the duration of the size exclusion run. Buffer subtraction was performed by averaging 50 frames either side of the peak. All subsequent data processing steps were performed using the ATSAS data analysis software 2.8.2. The program DATGNOM (57) was used to generate the pair distribution function [$P(r)$] for each isoform and to determine $D_{max}$ and $R_g$ from the scattering curves [I(q) vs. q] in an automatic, unbiased manner. Ab initio molecular envelopes for $Akt1^{DrLink}$ were computed by 10 iterative cycles of simulated annealing starting with a dummy atom model in DAMMIF (58). The models were aligned, averaged, and filtered using DAMAVER (59). The structure of $Akt1^{1-443}$ in complex with inhibitor VIII (PDB ID code 3O96) was compared with the scattering of $Akt1^{DrLink}$ using CRYSOL (60) and superimposed with the refined ab initio envelope using SUPCOMB (61). For $Akt1^{DA}$, rigid body modeling was performed using CORAL (27), with PDB ID code 1UNP (PH domain) and PDB ID code 4EKK (chain A; kinase domain) as the starting rigid body models. Linker residues were implemented in CORAL as dummy residues. Iterative runs of CORAL were performed in which the kinase domain was allowed to move, while the PH domain was fixed.

**Differential Scanning Fluorimetry.** The thermal stabilities of $Akt1^{WT}$, $Akt1^{DrLink}$, $Akt1^{DA}$, and their respective dephosphorylated species were measured by differential scanning fluorimetry (DSF). $Akt1^{DrLink}$ S473D, in vitro phosphorylated on T308, was also measured. Samples contained 0.1 mg/mL of protein in 20 mM Tris pH 8.0, 100 mM NaCl, and 1 mM TCEP. Samples were measured in triplicate using a BioRad iQ5 Multicolor Real-Time PCR Detection System.

**Fluorescence Anisotropy.** The affinity of the kinase and PH domains for each other was determined by fluorescence anisotropy, using Atto488-labeled $Akt1^{PH}$. Briefly, $Akt1^{1-120}$ harboring the mutation T101C was purified as described previously (15). The protein was incubated for 3 h at room temperature (RT) with a twofold excess of Atto488 maleimide (Atto-Tec), quenched with 0.5% (vol/vol) β-mercaptoethanol, and purified by size exclusion chromatography on a Superdex 75 10/30 column equilibrated in 20 mM Tris, pH 7.4, 300 mM NaCl, 1 mM TCEP, and 1% (vol/vol) glycerol. Fractions containing monomeric, labeled $Akt1^{PH}$ were collected and concentrated. The final concentration of $Akt1^{PH}$ was determined to be 15.5 μM at 280 nm, or 7.3 μM using the extinction coefficient of the dye, indicating ∼50% labeling efficiency. Concentrated $Akt1^{KD}$ was incubated with 100 nM Atto488-$Akt1^{PH}$ in 20 mM Tris, pH 7.4, 100 mM NaCl, 1 mM TCEP, and 1% (vol/vol) glycerol. The binding curve was constructed by making serial dilutions of $Akt1^{KD}$ in the same buffer containing 100 nM Atto488-$Akt1^{PH}$. Measurements were made with a Perkin-Elmer LS50B fluorimeter ($\lambda_{ex}$ = 502 nm, $\lambda_{em}$ = 520 nm) at 25 °C. For each data point, 50 measurements, each with an integration time of 1 s, were averaged. Each experiment was performed three times.

**HDX-MS.** HDX-MS experiments were similar to those described in refs. 34–36. In brief, HDX experiments were conducted in 50-μL reactions with a final concentration of 400 nM for $Akt1^{DA}$ dephos./$Akt1^{DrLink}$ dephos., 400 nM for $Akt1^{DrLink}$ pT308 S473D, 291 nM for $Akt1^{DA}$ mutant, and 260 nM for $Akt1^{DrLink}$. Eight conditions were tested: $Akt1^{DA}$ (*i*) alone and (*ii*) with lipid vesicles [20% cholesterol, 30% phosphatidylcholine (PC), 15% phosphatidylserine (PS), 35% phosphatidylethanolamine (PE), and 5% $PIP_3$] present at 400 μM final concentration; $Akt1^{DrLink}$ (*iii*) alone, (*iv*) with lipid vesicles containing $PIP_3$ (20% cholesterol, 30% PC, 15% PS, 35% PE, and 5% $PIP_3$) present at 400 μM final concentration and (*v*) with lipid vesicles containing no $PIP_3$ (20% cholesterol, 30% PC, 20% PS, and 35% PE) present at 400 μM final concentration; (*vi*) $Akt1^{DrLink}$ dephos. alone; (*vii*) $Akt1^{DA}$ dephos. alone; and (*viii*) $Akt1^{DrLink}$ pT308 S473D alone. For conditions with vesicles, protein was allowed to incubate with lipid vesicles for 2 min before initiation of deuterium exchange. Deuterium exchange was initiated by the addition of 40 μL to 45 μL of deuterated buffer [10 mM Hepes pH 7.5, 100 mM NaCl, 98% (vol/vol) $D_2O$]. Exchange was carried out for four (3 s, 30 s, 300 s, and 3,000 s at 23 °C) or five time points (with an additional 3-s time point on ice) and terminated by the addition of 20 μL of ice-cold quench buffer (2 M guanidine HCl, 3% formic acid). Samples were immediately frozen in liquid nitrogen and stored at −80 °C.

Protein samples were rapidly thawed and injected onto an ultra-performance liquid chromatography (UPLC) system at 2 °C. Protein was run over two immobilized pepsin columns (porosyme, 2-3131-00; Applied Biosystems) at 10 °C and 2 °C at 200 μL/min for 3 min, and peptides were collected onto a VanGuard precolumn trap (Waters). The trap was subsequently eluted in line with an Acquity 1.7-μm particle, 100 × 1 $mm^2$ C18 UPLC column (Waters), using a gradient of 5 to 36% B (buffer A 0.1% formic acid, buffer B 100% acetonitrile) over 16 min. Mass spectrometry experiments were performed on an Impact II TOF (Bruker) acquiring over a mass range from 150 *m/z* to 2,200 *m/z* using an electrospray ionization source operated at a temperature of 200 °C and a spray voltage of 4.5 kV. Peptides were identified using data-dependent acquisition methods following tandem MS/MS experiments (0.5-s precursor scan from 150 *m/z* to 2,000 *m/z*; 12 0.25-s fragment scans from 150 *m/z* to 2,000 *m/z*). MS/MS datasets were analyzed using PEAKS7 (PEAKS), and a false discovery rate was set at 1% using a database of purified proteins and known contaminants.

HD-Examiner Software (Sierra Analytics) was used to automatically calculate the level of deuterium incorporation into each peptide. All peptides were manually inspected for correct charge state and presence of

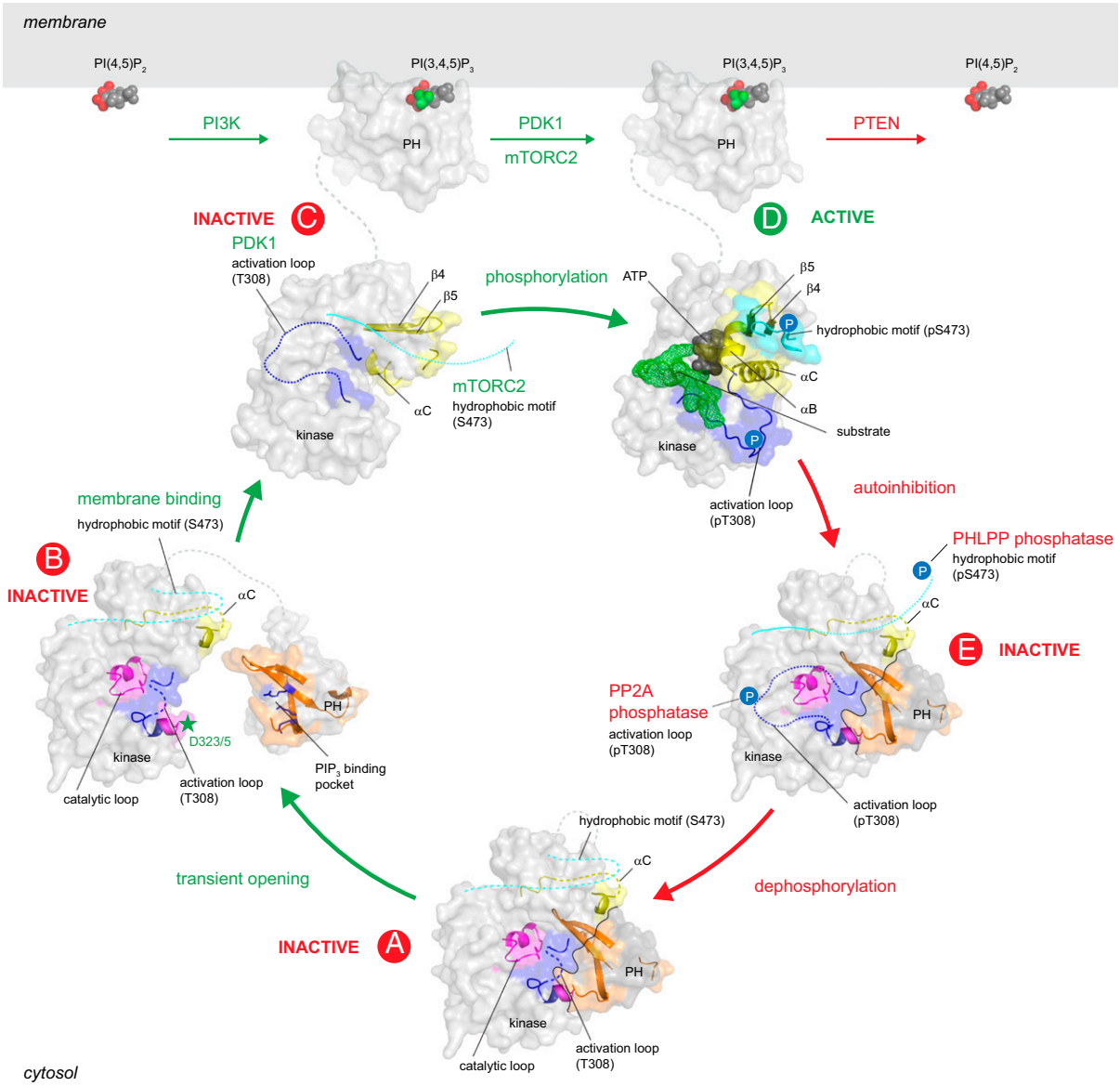


**Fig. 5.** Stepwise activation of Akt at membranes and inactivation in the cytosol. Autoinhibited Akt is characterized by a PH-in conformation in which its $PIP_3$-binding site is sequestered by interaction with the kinase domain and its PH domain blocks substrate binding. At equilibrium, a small fraction of Akt in which the interface has relaxed to a more open conformation is able to sample the membrane for $PIP_3$ or $PI(3,4)P_2$, engagement of which leads to displacement of the PH domain from the kinase domain and concomitant exposure of the two regulatory phosphorylation sites in the activation loop (T308) and hydrophobic motif (S473). Phosphorylation of these sites by PDK1 (T308) and mTORC2 (S473) leads to conformational changes in the kinase domain, docking of the phosphorylated motifs, and the high-affinity binding of $ATP.Mg^{2+}$. As long as Akt remains membrane-bound, the phosphorylated residues are protected from dephosphorylation by the high-affinity interaction with $ATP.Mg^{2+}$. However, upon termination of the $PIP_3$ signal, dissociation from the membrane rapidly leads to inhibition of the kinase domain by the PH domain and concomitant exposure of the activation loop and hydrophobic motif for dephosphorylation. In this way, Akt activation and activity are acutely restricted to the membrane, while it is inactivated in the cytosol. States A and E are modeled on the structure of Akt in complex with inhibitor VIII (PDB ID code 3O96). Protected/deprotected residues in the PH domain are colored orange, and those on the kinase domain are blue (activation loop), magenta (catalytic loop), yellow (kinase N lobe), and cyan (C-terminal tail). The kinase domain in state D is taken from Akt in complex with a substrate peptide derived from GSK3β (green; PDB ID code 1O6K).

overlapping peptides. Deuteration levels were calculated using the centroid of the experimental isotope clusters. Results for these proteins are presented as relative levels of deuterium incorporation, and the only control for back-exchange was the level of deuterium present in the buffer (76.92 to 86.53%). The average error of all time points and conditions for each HDX project was 0.7% and 0.1 Da. Therefore, changes in any peptide at any time point greater than both 7% and 0.4 Da between conditions with a paired *t* test value of $P < 0.05$ was considered significant and used to generate Fig. 3. All deuterium exchange data for all experiments are shown in *SI Appendix*, Figs. S7, S8, and S12, with deuterium incorporation graphs for selected peptides highlighted in Fig. 3 shown in *SI Appendix*, Figs. S9 and S13.

**In Vitro Dephosphorylation of Akt1.** Akt1 was dephosphorylated in vitro using lambda phosphatase (made in-house). Briefly, Akt1 (0.375 μM) was incubated with 100 ng to 150 ng of lambda phosphatase in a 50-μL reaction at RT. Aliquots were taken at fixed time points, mixed with SDS loading buffer, and heat-inactivated at 95 °C for 2 min. Samples were blotted onto nitrocellulose membranes and blocked with 5% BSA in 1× TBS + 0.1% TWEEN 20, and phosphorylated Akt was detected with antibodies against pT308 or pS473 (#C31E5E and #193H12, respectively; Cell Signaling Technology). Data reported in Fig. 4 *B* and *C* were obtained by Western blotting of dephosphorylation reactions containing both full-length $Akt1^{3C}$ S473D and $Akt1^{KD}$ S473D. The blots were incubated simultaneously with mouse and

rabbit primary antibodies against pan-Akt and pT308, respectively, washed, and developed with IRdye-conjugated anti-mouse IgG (700 nm) and anti-rabbit IgG (800 nm) secondary antibodies (LI-COR). Fluorescence was measured on a LI-COR Odyssey CLx infrared imager. Data reported in Fig. 4 *E*, *F*, *H*, and *I* were obtained by developing Western blots with HRP-conjugated anti-rabbit IgG secondary antibody and ECL Select Western blotting detection reagent (Amersham). Chemiluminescence was measured on a Fusion FX7 Advance (Peqlab), and the phospho-Akt signal was quantitated in ImageJ. For dephosphorylation of S473, 0.375 μM Akt1 was incubated with sucrose-loaded vesicles containing 0 mol % $PIP_3$ or 5 mol % $PIP_3$ at a total lipid concentration of 0.5 mM (25 μM $PIP_3$). The statistical significance of the fitted values of tau or the offset (y0) was calculated with an *F* test.

**ACKNOWLEDGMENTS.** We acknowledge Dr. Dorothea Anrather in the Max F. Perutz Laboratories (MFPL) Mass Spectrometry Facility, Dr. Bart van Leer for beamline support on BM29 at ESRF, Grenoble, and Florian Pflug for statistical analysis. This work was funded by Austrian Science Fund Grant P 28135 (to T.A.L.), a University of Vienna Thesis Completion Fellowship (to I.L.), and Hertha Firnberg Postdoctoral Fellowship T 915 (to L.T.). J.E.B. is supported by a new investigator grant from the Canadian Institutes of Health Research (CIHR), and Natural Sciences and Engineering Research Council of Canada Discovery Research Grant NSERC-2014-05218.

1. Manning BD, Toker A (2017) AKT/PKB signaling: Navigating the network. *Cell* 169: 381–405.
2. Carpten JD, et al. (2007) A transforming mutation in the pleckstrin homology domain of AKT1 in cancer. *Nature* 448:439–444.
3. Lindhurst MJ, et al. (2011) A mosaic activating mutation in AKT1 associated with the Proteus syndrome. *N Engl J Med* 365:611–619.
4. Nellist M, et al. (2015) Germline activating AKT3 mutation associated with megalencephaly, polymicrogyria, epilepsy and hypoglycemia. *Mol Genet Metab* 114:467–473.
5. Lee JH, et al. (2012) De novo somatic mutations in components of the PI3K-AKT3-mTOR pathway cause hemimegalencephaly. *Nat Genet* 44:941–945.
6. Cho H, et al. (2001) Insulin resistance and a diabetes mellitus-like syndrome in mice lacking the protein kinase Akt2 (PKB beta). *Science* 292:1728–1731.
7. George S, et al. (2004) A family with severe insulin resistance and diabetes due to a mutation in AKT2. *Science* 304:1325–1328.
8. Fruman DA, et al. (2017) The PI3K pathway in human disease. *Cell* 170:605–635.
9. Alessi DR, et al. (1997) Characterization of a 3-phosphoinositide-dependent protein kinase which phosphorylates and activates protein kinase Bα. *Curr Biol* 7:261–269.
10. Sarbassov DD, Guertin DA, Ali SM, Sabatini DM (2005) Phosphorylation and regulation of Akt/PKB by the rictor-mTOR complex. *Science* 307:1098–1101.
11. Facchinetti V, et al. (2008) The mammalian target of rapamycin complex 2 controls folding and stability of Akt and protein kinase C. *EMBO J* 27:1932–1943.
12. Ebner M, Lucic I, Leonard TA, Yudushkin I (2017) PI(3,4,5)P3 engagement restricts Akt activity to cellular membranes. *Mol Cell* 65:416–431.e6.
13. Falasca M, Maffucci T (2012) Regulation and cellular functions of class II phosphoinositide 3-kinases. *Biochem J* 443:587–601.
14. Bunney TD, Katan M (2010) Phosphoinositide signalling in cancer: Beyond PI3K and PTEN. *Nat Rev Cancer* 10:342–352.
15. Thomas CC, Deak M, Alessi DR, van Aalten DM (2002) High-resolution structure of the pleckstrin homology domain of protein kinase B/Akt bound to phosphatidylinositol (3,4,5)-trisphosphate. *Curr Biol* 12:1256–1262.
16. Stokoe D, et al. (1997) Dual role of phosphatidylinositol-3,4,5-trisphosphate in the activation of protein kinase B. *Science* 277:567–570.
17. Balzano D, et al. (2015) Alternative activation mechanisms of protein kinase B trigger distinct downstream signaling responses. *J Biol Chem* 290:24975–24985.
18. Calleja V, et al. (2007) Intramolecular and intermolecular interactions of protein kinase B define its activation in vivo. *PLoS Biol* 5:e95.
19. Huang BX, Kim HY (2006) Interdomain conformational changes in Akt activation revealed by chemical cross-linking and tandem mass spectrometry. *Mol Cell Proteomics* 5:1045–1053.
20. Ananthanarayanan B, Fosbrink M, Rahdar M, Zhang J (2007) Live-cell molecular analysis of Akt activation reveals roles for activation loop phosphorylation. *J Biol Chem* 282:36634–36641.
21. Parikh C, et al. (2012) Disruption of PH-kinase domain interactions leads to oncogenic activation of AKT in human cancers. *Proc Natl Acad Sci USA* 109:19368–19373.
22. Calleja V, Laguerre M, Larijani B (2009) 3-D structure and dynamics of protein kinase B-new mechanism for the allosteric regulation of an AGC kinase. *J Chem Biol* 2:11–25.
23. Calleja V, Laguerre M, Parker PJ, Larijani B (2009) Role of a novel PH-kinase domain interface in PKB/Akt regulation: Structural mechanism for allosteric inhibition. *PLoS Biol* 7:e17.
24. Wu WI, et al. (2010) Crystal structure of human AKT1 with an allosteric inhibitor reveals a new mode of kinase inhibition. *PLoS One* 5:e12913.
25. Lapierre JM, et al. (2016) Discovery of 3-(3-(4-(1-Aminocyclobutyl)phenyl)-5-phenyl-3H-imidazo[4,5-b]pyridin-2-yl)pyridin -2-amine (ARQ 092): An orally bioavailable, selective, and potent allosteric AKT inhibitor. *J Med Chem* 59:6455–6469.
26. Ashwell MA, et al. (2012) Discovery and optimization of a series of 3-(3-phenyl-3H-imidazo[4,5-b]pyridin-2-yl)pyridin-2-amines: Orally bioavailable, selective, and potent ATP-independent Akt inhibitors. *J Med Chem* 55:5291–5310.
27. Petoukhov MV, et al. (2012) New developments in the program package for small-angle scattering data analysis. *J Appl Crystallogr* 45:342–350.
28. Milburn CC, et al. (2003) Binding of phosphatidylinositol 3,4,5-trisphosphate to the pleckstrin homology domain of protein kinase B induces a conformational change. *Biochem J* 375:531–538.
29. Lin K, et al. (2012) An ATP-site on-off switch that restricts phosphatase accessibility of Akt. *Sci Signal* 5:ra37.
30. Pouillon V, et al. (2003) Inositol 1,3,4,5-tetrakisphosphate is essential for T lymphocyte development. *Nat Immunol* 4:1136–1143.
31. Miller AT, et al. (2007) Production of Ins(1,3,4,5)P4 mediated by the kinase Itpkb inhibits store-operated calcium channels and regulates B cell selection and activation. *Nat Immunol* 8:514–521.
32. Jia Y, et al. (2008) Inositol trisphosphate 3-kinase B (InsP3KB) as a physiological modulator of myelopoiesis. *Proc Natl Acad Sci USA* 105:4739–4744.
33. Harrison RA, Engen JR (2016) Conformational insight into multi-protein signaling assemblies by hydrogen-deuterium exchange mass spectrometry. *Curr Opin Struct Biol* 41:187–193.
34. Vadas O, Jenkins ML, Dornan GL, Burke JE (2017) Using hydrogen-deuterium exchange mass spectrometry to examine protein-membrane interactions. *Methods Enzymol* 583:143–172.
35. Siempelkamp BD, Rathinaswamy MK, Jenkins ML, Burke JE (2017) Molecular mechanism of activation of class IA phosphoinositide 3-kinases (PI3Ks) by membrane-localized HRas. *J Biol Chem* 292:12256–12266.
36. Dornan GL, et al. (2017) Conformational disruption of PI3Kdelta regulation by immunodeficiency mutations in PIK3CD and PIK3R1. *Proc Natl Acad Sci USA* 114:1982–1987.
37. Yang J, et al. (2002) Molecular mechanism for the regulation of protein kinase B/Akt by hydrophobic motif phosphorylation. *Mol Cell* 9:1227–1240.
38. Kunkel MT, Ni Q, Tsien RY, Zhang J, Newton AC (2005) Spatio-temporal dynamics of protein kinase B/Akt signaling revealed by a genetically encoded fluorescent reporter. *J Biol Chem* 280:5581–5587.
39. Antal CE, Newton AC (2013) Spatiotemporal dynamics of phosphorylation in lipid second messenger signaling. *Mol Cell Proteomics* 12:3498–3508.
40. Chan TO, et al. (2011) Resistance of Akt kinases to dephosphorylation through ATP-dependent conformational plasticity. *Proc Natl Acad Sci USA* 108:E1120–E1127.
41. Lu S, et al. (2015) The mechanism of ATP-dependent allosteric protection of Akt kinase phosphorylation. *Structure* 23:1725–1734.
42. Yang J, et al. (2002) Crystal structure of an activated Akt/protein kinase B ternary complex with GSK3-peptide and AMP-PNP. *Nat Struct Biol* 9:940–944.
43. Endicott JA, Noble ME, Johnson LN (2012) The structural basis for control of eukaryotic protein kinases. *Annu Rev Biochem* 81:587–613.
44. Ubersax JA, Ferrell JE, Jr (2007) Mechanisms of specificity in protein phosphorylation. *Nat Rev Mol Cell Biol* 8:530–541.
45. Pearce LR, Komander D, Alessi DR (2010) The nuts and bolts of AGC protein kinases. *Nat Rev Mol Cell Biol* 11:9–22.
46. Hubbard SR (2004) Juxtamembrane autoinhibition in receptor tyrosine kinases. *Nat Rev Mol Cell Biol* 5:464–471.
47. Truebestein L, Elsner DJ, Fuchs E, Leonard TA (2015) A molecular ruler regulates cytoskeletal remodelling by the Rho kinases. *Nat Commun* 6:10029.
48. Nolen B, Taylor S, Ghosh G (2004) Regulation of protein kinases; controlling activity through activation segment conformation. *Mol Cell* 15:661–675.
49. Pittet D, Schlegel W, Lew DP, Monod A, Mayr GW (1989) Mass changes in inositol tetrakis- and pentakisphosphate isomers induced by chemotactic peptide stimulation in HL-60 cells. *J Biol Chem* 264:18489–18493.
50. Huang BX, Akbar M, Kevala K, Kim HY (2011) Phosphatidylserine is a critical modulator for Akt activation. *J Cell Biol* 192:979–992.
51. Warfel NA, Niederst M, Newton AC (2011) Disruption of the interface between the pleckstrin homology (PH) and kinase domains of Akt protein is sufficient for hydrophobic motif site phosphorylation in the absence of mTORC2. *J Biol Chem* 286:39122–39129.
52. Okuzumi T, et al. (2009) Inhibitor hijacking of Akt activation. *Nat Chem Biol* 5:484–493.
53. Han EK, et al. (2007) Akt inhibitor A-443654 induces rapid Akt Ser-473 phosphorylation independent of mTORC1 inhibition. *Oncogene* 26:5655–5661.
54. Gao T, Furnari F, Newton AC (2005) PHLPP: A phosphatase that directly dephosphorylates Akt, promotes apoptosis, and suppresses tumor growth. *Mol Cell* 18:13–24.
55. Andjelković M, et al. (1996) Activation and phosphorylation of a pleckstrin homology domain containing protein kinase (RAC-PK/PKB) promoted by serum and protein phosphatase inhibitors. *Proc Natl Acad Sci USA* 93:5699–5704.
56. Resjö S, et al. (2002) Protein phosphatase 2A is the main phosphatase involved in the regulation of protein kinase B in rat adipocytes. *Cell Signal* 14:231–238.
57. Petoukhov MV, Konarev PV, Kikhney AG, Svergun DI (2007) ATSAS 2.1–Towards automated and web-supported small-angle scattering data analysis. *J Appl Crystallogr* 40:S223–S228.
58. Franke D, Svergun DI (2009) DAMMIF, a program for rapid ab-initio shape determination in small-angle scattering. *J Appl Crystallogr* 42:342–346.
59. Volkov VV, Svergun DI (2003) Uniqueness of ab initio shape determination in small-angle scattering. *J Appl Crystallogr* 36:860–864.
60. Svergun D, Barberato C, Koch MHJ (1995) CRYSOL–A program to evaluate X-ray solution scattering of biological macromolecules from atomic coordinates. *J Appl Crystallogr* 28:768–773.
61. Kozin MB, Svergun DI (2001) Automated matching of high- and low-resolution structural models. *J Appl Crystallogr* 34:33–41.